Article

A Novel Molecular Assembly of a Cobalt–Sulfate Coordination Polymer and Melamine: A Manifestation of Magnetic Anisotropy

Ignacio Bernabé Vírseda, Shiraz Ahmed Siddiqui, Alexander Prado-Roller, Michael Eisterer, and Hidetsugu Shiozawa*
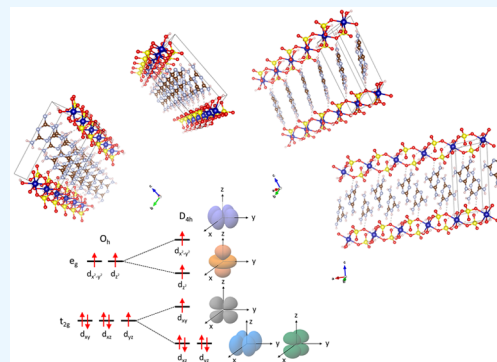
Read Online

ACCESS | Metrics & More | Article Recommendations | Supporting Information

ABSTRACT: A novel molecular assembly of a cobalt–sulfate coordination polymer and melamine is synthesized under acidic conditions. Bar-shaped pink monocrystals as long as 1 mm are found to align along magnetic field lines in the proximity of a strong magnet. Magnetometry shows no hysteresis at temperatures down to 2 K but instead magnetic anisotropy and antiferromagnetic coupling. X-ray diffraction on a single crystal reveals that the cobalt–sulfate chains are along the shortest lattice vector or the crystal's long axis. The crystal alignment along the magnetic flux can be attributed to single-ion anisotropy that results in longitudinal antiferromagnetic coupling along the chain. Both structurally and magnetically isotropic crystals of metal–organic hybrid materials can be highly useful as elemental components in magneto-optics.

INTRODUCTION

Coordination polymers are molecular arrays composed of metal ions and bridging organic or inorganic ligands.[1−3] Combinations of predesigned organic ligands and metal centers with versatile coordination geometries enable a variety of one-, two-, or three-dimensional lattice structures including porous metal–organic frameworks (MOFs). Because of their diverse properties, coordination polymers are promising materials for energy transfer, gas storage and separation, catalysis, electronic, optical, and magnetic applications.[4−6]

Molecular magnets are a class of magnetic materials based on organic molecules, coordination compounds, or hybrids. Coordination polymers as molecular magnets can exhibit various magnetic properties due to directional magnetic coupling among magnetic metals through low-dimensionally arranged molecular units. They are vital for understanding of the fundamentals of magnetic coupling and the magneto–structure correlation. In particular, those with higher critical temperatures could be useful in high-density magnetic information storage and quantum computation.[7−9]

In this contribution, a novel molecular framework of a cobalt–sulfate coordination polymer and melamine is synthesized. Melamine is a rich source of hydrogen bonds. Its molecular symmetry and skeleton rigidity (see Figure 1A) are useful for constructing supramolecular frameworks,[10] while the use of melamine is not very common in coordination chemistry because of the low solubility in organic solvents.[11] Synthesis parameters are optimized to yield millimeter-long single crystals. X-ray diffraction reveals layers of cobalt–sulfate chains packed with stacks of melamine by hydrogen bonding.

Crystals align along the magnetic flux at room temperature like compass needles, making this polymer a good candidate for a molecular magnet. Magnetometry reveals no hysteresis but instead antiferromagnetic coupling at low temperatures and magnetic anisotropy. The weak but directional response of bar-shaped crystals to the external magnetic field can be attributed to the single-ion anisotropy that results in longitudinal antiferromagnetic coupling along the chain.

RESULTS AND DISCUSSION

Synthesis. Unless otherwise noted, all crystals (referred to as CoS-M) have been synthesized by mixing an aqueous solution of $CoSO_4 \cdot 7H_2O$ and an acetic acid solution of melamine, followed by heating the mixture in a sealed glass vial.

The table in Figure 1B illustrates the quality of crystals synthesized at various concentrations of $CoSO_4 \cdot 7H_2O$ and melamine at 70 °C, which ensures the solubility of melamine in acetic acid. In each case, 1 mL of the aqueous solution of $CoSO_4 \cdot 7H_2O$ was placed in a 10 mL glass vial and then 3 mL of the acetic acid solution of melamine was added. The concentrations of $CoSO_4 \cdot 7H_2O$ in water tested are $\rho_{Co} = 0.025$
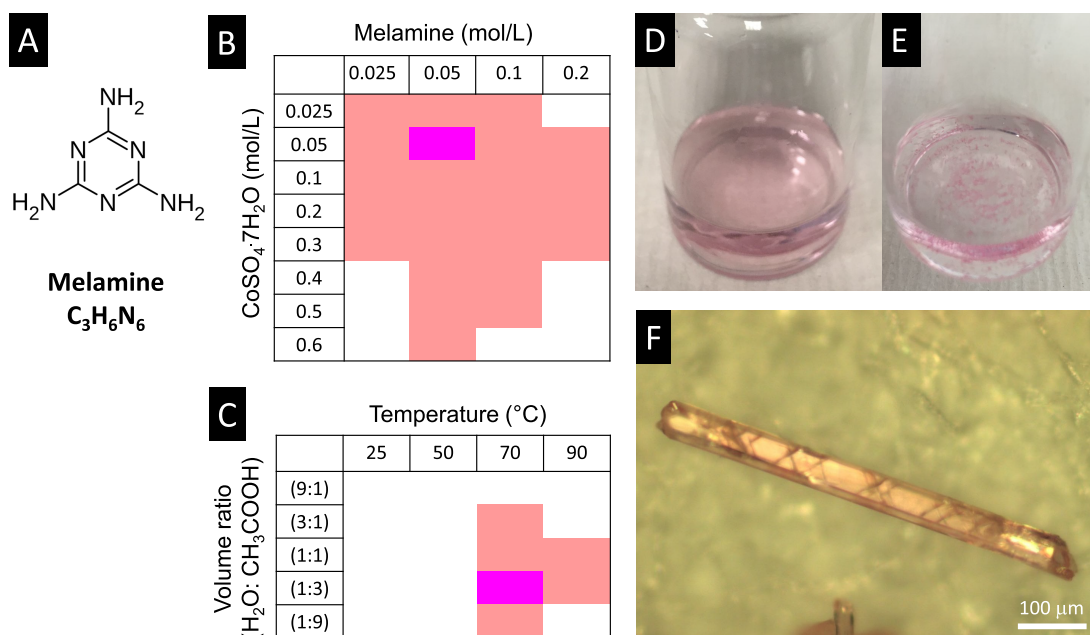
Figure 1. (A) The structure of melamine. (B) Crystal growth at 70 °C at various concentrations of CoSO$_4$·7H$_2$O and melamine. Purple and pink denote the best and marginal crystal quality, respectively, and white denotes no crystal formation. (C) Crystal growth at different temperatures and water to acetic acid ratios. (D and E) Photographs of the solution in the glass vial taken just as prepared and 3 h later, respectively. (F) Optical micrographs of CoS-M crystals synthesized under optimal conditions: 70 °C, (ρ_{Co}, $\rho_{melamine}$) = (0.05 mol/L, 0.05 mol/L), and a water-to-acetic acid volume ratio of 1:3.

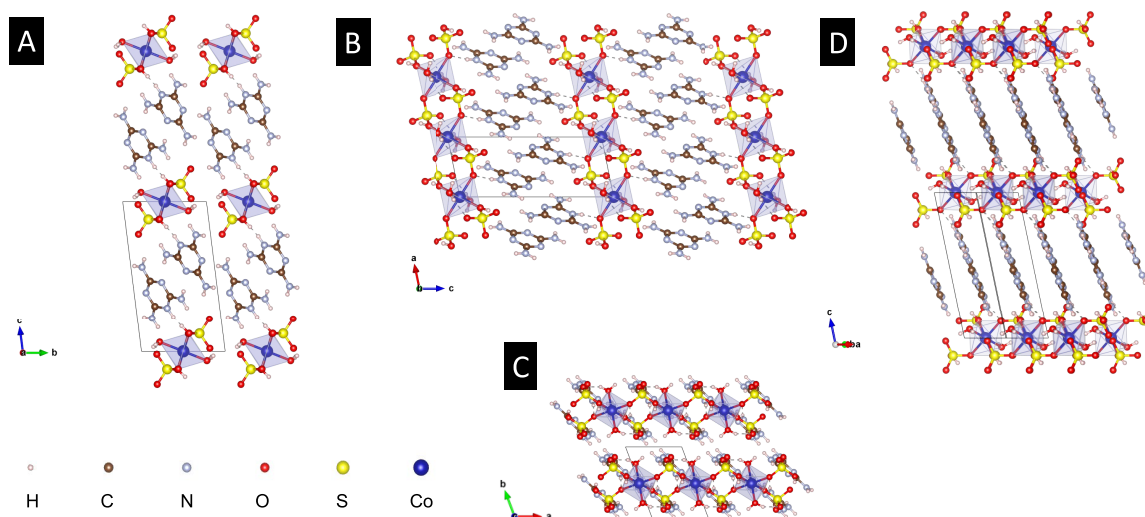**Figure 2.** (a–D) The lattice structures of CoS-M viewed along axes a, b, c, and [1, −1, 0]. The space group is $\overline{P}1$. The lattice parameters are a = 5.3182 Å, b = 7.2591 Å, c = 12.5757 Å, α = 93.3633°, β = 99.5922°, and γ = 109.6577°.

and 0.05, 0.1, 0.2, 0.4, 0.5, 0.6, and 0.8 mol/L, and the concentrations of melamine in acetic acid are $\rho_{Melamine}$ = 0.025, 0.05, 0.1, and 0.2 mol/L. Purple and pink denote the best and marginal crystal quality, respectively, and white denotes no crystal formation. At ρ_{Co} = 0.8 mol/L, no crystals were formed. The largest crystals, approximately 500 μm long, as in Figure 1F, are obtained at (ρ_{Co}, $\rho_{Melamine}$) = (0.05 mol/L, 0.05 mol/L). When the sample is under the same conditions but pressurized in an autoclave (1.38 bar), the crystal length reaches around 1000 μm (see the Supporting Information (SI) for more details on the hydrothermal synthesis).

The higher concentrations hinder the formation of the crystals, possibly due to the increased ionic strength of both cations Co(II) and anions SO$_4^{2-}$, which decreases the mobility and diffusion of the reactants and consequently affects the coordination between metal ions and the ligand.[12] At the low concentrations, the mobility is high but nucleation does not occur.[13]

Figure 1C shows the quality of crystals formed at different temperatures and volume ratios of water and acetic acid. Temperatures tested are 25, 50, 70, and 90 °C, and volume ratios of water and acetic acid are (water/acetic acid) = (9:1),
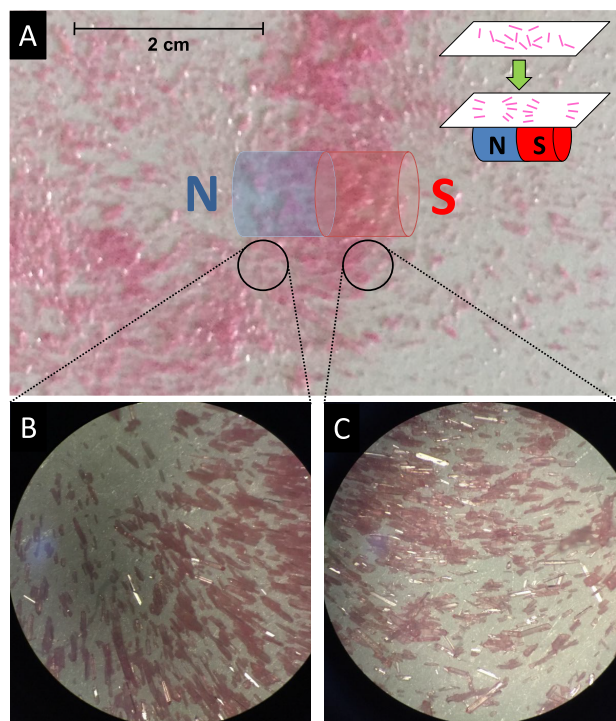
Figure 3. (A−C) Optical micrographs of the alignment of CoS-M crystals along magnetic fields. The inset in panel A shows a schematic diagram of CoS-M crystals dispersed on a paper and then subjected to the magnetic field of a cylindrical NdFeB magnet (VMMSH, Magsy, Czech Republic; diameter of 10 mm and length of 20 mm) underneath the paper.
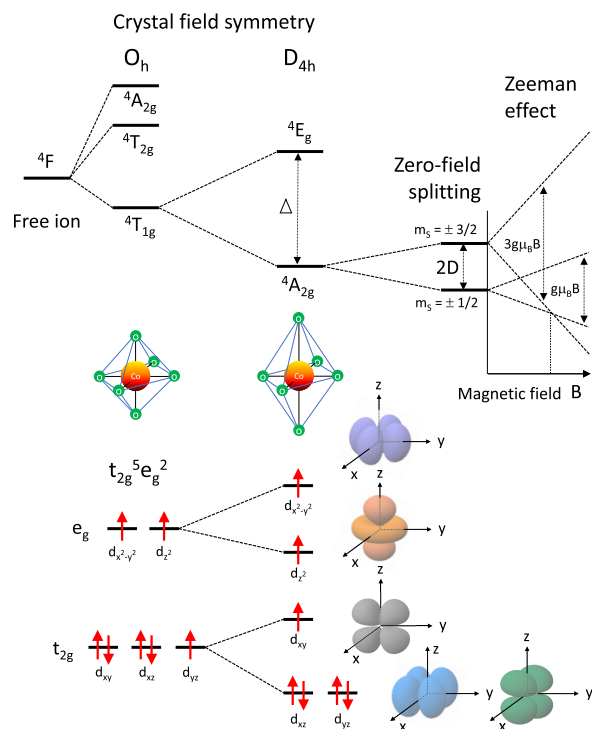

Figure 4. Energy diagram for a high-spin Co(II) ion in an axially distorted octahedral geometry.

(3:1), (1:1), (1:3), and (1:9). The total volume of the solution was 4 mL.

The best-quality crystals grow at 70 °C and (1:3). At lower temperatures, melamine does not dissolve, as concluded in the solubility tests (see SI-1). As a result, no crystals are formed. This indicates that melamine plays a vital role in the formation of the crystal, ensuring its presence in the solid structure. At 90 °C, marginal quality crystals grow only at (1:1) and (1:3). A high temperature promotes the diffusion of reactants and consequently the nucleation. On the other hand, it hinders relaxation steps required for crystal formation.[14,15] Therefore, temperatures higher than 70 °C are not optimal for the growth of CoS-M crystals.

As for the influence of the volume ratio, (water/acetic acid) = (1:3) is optimal. In the solvent with excess water (or acetic acid), melamine (or $CoSO_4 \cdot 7H_2O$) does not fully dissolve.

Panels D and E in Figure 1 are the photographs of the solution in the glass vial taken just as prepared and 3 h later, respectively. The initial solution has pink color (Figure 1E) and a pH scale of 1.35 ± 0.06. The confidence interval was estimated as the 95% confidence interval of a "t of Student" distribution for which five simultaneous measurements were conducted. In approximately 30 min, pink dots appear on the bottom surface, and in 3 h the solution turns colorless as CoS-M crystals stop growing (Figure 1F). The pH scale at this point is 0.64 ± 0.08.

The fact that the solution gets more acidic after the formation of CoS-M may be related to the incorporation of H_2O molecules into the crystals, which increases the concentration of acetic acid in the solution and consequently the concentration of H^+.

Structure Determination. Single-crystal X-ray diffraction reveals that CoS-M is a coordination polymer that consists of cobalt cations, sulfate anions, water and melamine, as shown in Figure 2. The empirical formula of CoS-M is $C_6H_{20}CoN_{12}O_{10}S_2$. To the best of our knowledge, this structure has not been previously reported, and only a similar one was reported (CCDC 689784).[10] The crystal is composed of cobalt−sulfate chains along the a-axis in which adjacent cobalt cations are bridged by two HSO_4^{-1} anions through Co−O bonds. Two H_2O molecules are also coordinated to the cobalt by their oxygen through Co−O bonds (2.08 Å). Each cobalt ion lies in an octahedral coordination geometry. The cobalt−sulfate chains lying in the (001) plane establish N−H⋯O bonds with melamine molecules, which are arranged in a zigzag fashion approximately within the (1 1 2) plane or facing the [2 2 1] direction. Importantly, the direction of the Co−S chains (axis a) was found to be along the long axis of the crystal.

Magnetism. The crystal's orientations are susceptible to an external magnetic field. When exposed to strong magnetic fields of a neodymium magnet, the long axis of the crystal becomes aligned along the field direction, as shown in Figure 3. This means that the Co−S chains are aligned along the magnetic field, as the chain axis is along the crystal's long axis. This longitudinal spin alignment is somewhat against the intuitive view that spins are aligned perpendicular to the chain axis and suggests the presence of magnetic anisotropy, which plays a decisive role in the orientation of crystals in a magnetic field.

The electronic configuration of divalent cobalt ion, Co(II), is [Ar] $3d^7$. The ligand field strength determines the splitting between the t_{2g} and e_g orbitals in an octahedral geometry. In a weak ligand field, the configuration is $t_{2g}^5 e_g^2$, resulting in a high spin state with total spin $S = 3/2$. The ground-state term of this
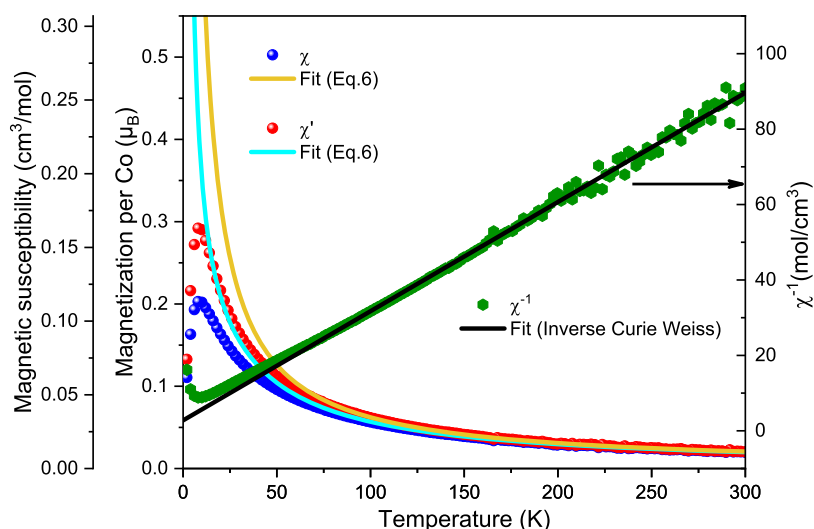
Figure 5. Magnetic susceptibility χ (solid blue circles), $\chi' = (\chi^{-1} + \theta/C)^{-1}$ (solid red circles), and the inverse magnetic susceptibility $1/\chi$ (solid green hexagons) of CoS-M crystals measured in a magnetic field of 1 T in the temperature range of 2−300 K. The curves of best fit obtained for χ and χ' in the temperature range of 100−300 K are extrapolated and plotted in cyan and orange, respectively, over the whole temperature range. The line of best fit obtained for $1/\chi$ in the temperature range of 150−300 K is extrapolated and plotted over the whole temperature range.
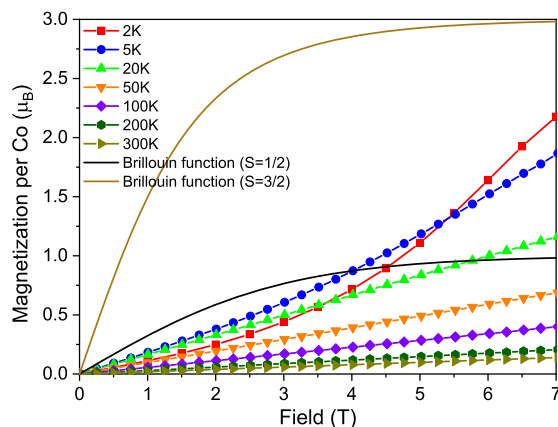

Figure 6. Magnetization isotherms measured at 2, 5, 20, 50, 100, 200, and 300 K.

quartet state is $^4T_{1g}$. In a strong ligand field, the configuration is $t_{2g}^6 e^1$, i.e., a low-spin state with total spin $S = 1/2$. The ground-state term of this singlet state is ^2E_g.[16]

A perfect octahedral coordination geometry O_h is hard to realize, and in most cases the octahedron is axially distorted to a tetragonal D_{4h} geometry. As shown in Figure 4, an axial elongation causes a splitting of the t_{2g} level, namely, the d_{xz} and d_{yz} orbitals move to a lower energy and the d_{xy} orbital moves to a higher energy. The e_g level splits into low-energy d_{z^2} and high-energy $d_{x^2-y^2}$. The corresponding term symbols for the ground and first excited states are $^4A_{2g}$ and ^4E_g, respectively, and are split by energy Δ. The $^4A_{2g}$ state further splits into two Kramers doublets, $m_s = \pm1/2$ and $\pm3/2$, as a result of spin−orbit coupling, with the zero-field splitting (ZFS) energy denoted by D in Figure 4. The ground state is $m_s = \pm1/2$ for $D > 0$ and $m_s = \pm3/2$ for $D < 0$.

Figure 5 shows the magnetic susceptibility χ (solid blue circles) and the inverse magnetic susceptibility $1/\chi$ (solid green hexagons) of CoS-M crystals measured in a magnetic field of 1 T in the temperature range of 2−300 K. No hysteresis was observed between the zero-field cooled and field

cooled data. See the SI for the χT plot and the AC susceptibility.

At high temperatures, the susceptibility follows the Curie−Weiss law $\chi = C/(T − \theta)$ where C is the Curie constant and θ the Weiss temperature. Using the inverse Curie−Weiss relation, the curve of best fit (the cyan curve in Figure 5) was obtained in the temperature range of 150−300 K with $C = 3.45$ cm^3 mol^{-1} K) and $\theta = -9.53$ K. The Curie constant is in agreement with the values for high-spin Co(II) in an octahedral environment ($C = 2.8-3.4$ cm^3 mol^{-1} K) reported in literature.[17−27] The corresponding effective magnetic moment is $\mu_{eff} = (8C)^{1/2} = 5.25$. The negative Weiss temperature suggests an antiferromagnetic coupling, likely between the nearest neighbor spins of the CoS chains (see Figure 7). This is consistent with the deviation of χ downward from the Curie−Weiss law at temperatures below 150 K, leading to the peak at 8 K.

In order to further evaluate the spin ground state by taking the zero-field splitting (ZFS) (D in Figure 4) into account, we use the following spin Hamiltonian:[16]

$$\hat{H} = D[\hat{S}_z^2 - 1/3S(S+1)] + g_{\parallel}\mu_B B_z \hat{S}_z + g_{\perp}\mu_B(B_x\hat{S}_x + B_y\hat{S}_y)$$

$$(1)$$

where D is the ZFS parameter; $\hat{S}_x$, $\hat{S}_y$, and $\hat{S}_z$ represent spin operators; S is the total spin quantum number; B_x, B_y, and B_z are the three scalar components for the external magnetic field; $g_{\parallel}$ and $g_{\perp}$ are the g-tensors in the directions parallel and perpendicular to the z-axis, respectively,; and μ_B is the Bohr magneton. The second term in the expression is the spin Zeeman term.

The magnetic susceptibility in the parallel direction ($\chi_{\parallel}$) and that in the perpendicular direction ($\chi_{\perp}$) are derived as[28−41]

$$\chi_{\parallel} = \frac{N\mu_B^2}{4kT}g_{\parallel}^2 F_{D\parallel}$$

$$(2)$$

$$\chi_{\perp} = \frac{N\mu_B^2}{4kT}g_{\perp}^2 F_{D\perp}$$
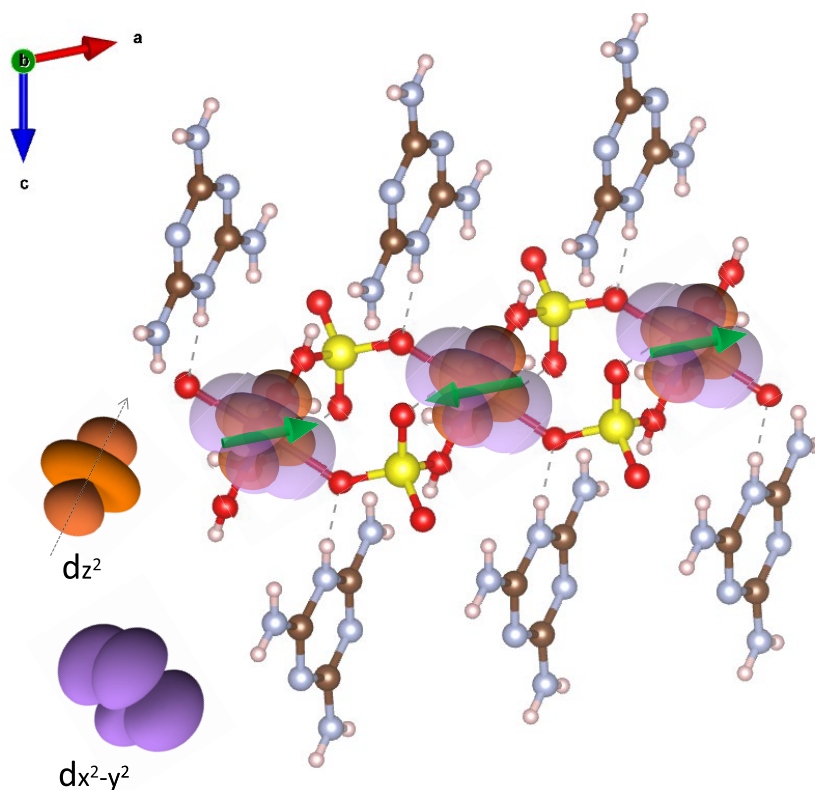
$$(3)$$

Figure 7. Co 3d$_{z^2}$ and 3d$_{x^2-y^2}$ orbitals with the quantization axis along the elongation direction of the octahedral ligand overlaid on the cobalt−sulfate coordination polymer lattice viewed along axis b. The green arrows represent cobalt spins antiferromagnetically coupled to one another and longitudinally aligned along the polymer chain axis.

where

$$F_{D\parallel} = \frac{1 + 9\exp\left(-\frac{D}{kT}\right)}{1 + \exp\left(-\frac{D}{kT}\right)} \tag{4}$$

$$F_{D\perp} = \frac{4 + 6\frac{kT}{D}\left[1 - \exp\left(-\frac{D}{kT}\right)\right]}{1 + \exp\left(-\frac{D}{kT}\right)} \tag{5}$$

N is the Avogadro constant, k is the the Boltzmann constant, and T is temperature.

The averaged magnetic susceptibility is given as

$$\chi_{\text{ave.}} = \frac{\chi_{\parallel} + 2\chi_{\perp}}{3} \tag{6}$$

We evaluate both χ and $\chi' = (\chi^{-1} + \theta/C)^{-1}$, namely, the susceptibility data with and without the Weiss molecular field term, which are plotted respectively as solid blue and red circles in Figure 5. The best fit for χ (orange curve in Figure 5) is obtained in the temperature range of 100−300 K, which gives $D = 5.2 \pm 0.49$ meV (= 42.1 ± 3.95 cm^{-1}), and $g_{\text{ave.}} = g_{\parallel} = g_{\perp} = 2.399 \pm 0.006$. The best fit for χ' (cyan curve in Figure 5) obtained in the same temperature range leads to $D = 0.97 \pm 0.76$ meV (= 7.8 ± 6.12 cm^{-1}) and $g_{\text{ave.}} = g_{\parallel} = g_{\perp} = 2.405 \pm 0.007$. The zero-field splitting energy evaluated from χ' is approximately five-times smaller than that evaluated from χ. As the Hamiltonian in eq 5 takes no exchange coupling into account, fitting χ' should provide a better estimate of the upper limit of D.

The zero-field splitting energies D reported for cobalt complexes are in the range from −38 to +73 cm^{-1} when the coordination numbers are 5 and 4 and from +25 to +83 cm^{-1} when the coordination number is 6.[42,43] $D = 0.97 \pm 0.76$ meV (= 7.8 ± 6.12 cm^{-1}) obtained here from the χ' is very small, approximately the thermal energy at 1 K. This means that in the temperature range of 100−300 K the zero-field splitting contributes to only a minor or no deviation from the S = 3/2 ground state.

Figure 6 shows the magnetization isotherms measured in fields up to 7 T at 2, 5, 20, 50, 100, 200, and 300 K. The low-temperature magnetism exceeds the saturation level (1.0 μ_B/Co) of the Brillouin function for S = 1/2, supporting the S = 3/2 ground state at 2 K. The magnetization curve deviates significantly from the Brillouin function for paramagnetism and exhibits a sigmoidal shape. See the SI for the magnetization isotherms of roughly aligned crystals measured in fields up to 9 T both parallel and normal to the dominant crystal orientation.

The magnetic moment reaches a value of 2.17 μ_B at 7 T and seems to coincide with the saturation level (3.0 μ_B/Co) for S = 3/2 in higher fields. The Zeeman energy in weak magnetic fields is proportional to ±(1/2)$g\mu_B B$ for $m_S = \pm 1/2$ and ±(3/2)$g\mu_B B$ for $m_S = \pm 3/2$.

The level crossing of the ground and first excited level separated by $D = 0.97 \pm 0.76$ meV may occur in a magnetic field of ≥17 T, which is much higher than the measured magnetic field range. Additionally, this small zero-field splitting is visible only at temperatures below 1 K. Furthermore, the magnetization curve at 2 K is smaller than the Brillouin function for S = 1/2 in fields below 4.5 T. Hence, the

sigmoidal magnetization curve can be attributed to the antiferromagnetic coupling of 3/2 spins in the Co−S chain.

As shown in Figure 3, the Co−S chains tend to become aligned along the magnetic field. This means that the spins are aligned along the chain and antiferromagnetically coupled one another, as depicted by the green arrows in Figure 7.

Now, we discuss mechanisms for the antiferromagnetic coupling. As shown in Figure 4, the three upper Co 3d orbitals, namely, $3d_{xy}$, $3d_{z^2}$, and $3d_{x^2-y^2}$ are half-filled and hence spin-polarized. The three spins are aligned one another according to Hund's rule. The lobes of the Co $3d_{z^2}$ and $3d_{x^2-y^2}$ orbitals are along the Co−O ligands, while the $3d_{xy}$ orbital lies off the ligand. In Figure 7, half-filled Co $3d_{z^2}$ and $3d_{x^2-y^2}$ orbitals with the quantization axis along the elongation direction of the octahedral ligand are superposed onto the lattice. The distance between the nearest-neighbor cobalt atoms is 5.32 Å, which is too far for direct exchange. The superexchange coupling through the Co−O−S bonds with an angle of 133° may favor antiferromagnetic coupling between spins of the cobalt d orbital and the oxygen p orbital. However, the sp³ hybrid orbitals of sulfur in HSO_4 have no favored exchange and should accommodate antiferromagnetically coupled spins in order to realize the antiferromagetic coupling of the adjacent cobalt ions. Hence, the antiferromagnetic coupling between cobalt atoms can be attributed to more elaborate interactions through super-exchange via HSO_4, whose sign depends largely on the bonding environment but has been reported to be antiferromagnetic in many metal sulfates and related materials.

Finally, the origin of the longitudinal spin orientation could be the single-ion anisotropy, anisotropic diamagnetism due to the molecular orientation, or the demagnetizing field due to the crystal's anisotropic shape. All melamine molecules face the [2 2 1] direction. Their aromatic rings exhibit anisotropic diamagnetism, which is the greatest when the rings face the field direction. The resulting demagnetizing field should favor the [2 2 1] direction along the field, but the crystals are aligned so as to make the [1 0 0] direction parallel to the field direction. In turn, the demagnetizing field for a typical crystal shape, e.g., $625 \times 50 \times 50 \ \mu m$ as in Figure 1F, does not exceed 20 mT, which is negligibly weak. Hence, the longitudinal orientation of the cobalt spins can be attributed to the single-ion anisotropy.

CONCLUSION

A cobalt−sulfate coordination polymer and melamine are assembled to form millimeter-long magnetic monocrystals. X-ray diffraction on a single crystal reveals that the cobalt−sulfate chains are along the crystal's long axis. Magnetometry evidences the longitudinal antiferromagnetic coupling of cobalt spins. As a result of the single-ion magnetic anisotropy, these magnetic crystals are aligned along magnetic field lines, which can be highly useful in magneto-optics.

ASSOCIATED CONTENT

ⓈⒾ Supporting Information

The Supporting Information is available free of charge at https://pubs.acs.org/doi/10.1021/acsomega.2c07556.

Experimental details, synthesis details, chemical and thermal stability, χ-plot, AC magnetic susceptibility, and anisotropy of the magnetic susceptibility (PDF)

Accession Codes

CCDC 2173264 contains the supplementary crystallographic data for this paper. These data can be obtained free of charge from The Cambridge Crystallographic Data Centre via www.ccdc.cam.ac.uk/structures.

AUTHOR INFORMATION

Corresponding Author

Hidetsugu Shiozawa − *J. Heyrovsky Institute of Physical Chemistry, Czech Academy of Sciences, 182 23 Prague, Czech Republic; Faculty of Physics, University of Vienna, 1090 Vienna, Austria;* ⓞ orcid.org/0000-0003-0603-2508; Email: hidetsugu.shiozawa@univie.ac.at, hide.shiozawa@jh-inst.cas.cz

Authors

Ignacio Bernabé Vírseda − *J. Heyrovsky Institute of Physical Chemistry, Czech Academy of Sciences, 182 23 Prague, Czech Republic;* Present Address: Departamento de Ingenieria Química Industrial y Medio Ambiente, Universidad Politécnica de Madrid, E.T.S.I. Industriales, 28006 Madrid, Spain

Shiraz Ahmed Siddiqui − *Faculty of Physics, University of Vienna, 1090 Vienna, Austria*

Alexander Prado-Roller − *Department of Inorganic Chemistry, University of Vienna, 1090 Vienna, Austria*

Michael Eisterer − *Atominstitut, TU Wien, 1020 Vienna, Austria;* ⓞ orcid.org/0000-0002-7160-7331

Complete contact information is available at:
https://pubs.acs.org/10.1021/acsomega.2c07556

REFERENCES

(1) Lehn, J.-M. *Supramolecular Chemistry: Concepts and Perspectives*; Wiley, 1995.

(2) Robson, R. A net-based approach to coordination polymers f. *J. Chem. Soc., Dalton Trans.* **2000**, 3735−3744.

(3) Biradha, K.; Ramanan, A.; Vittal, J. J. Coordination Polymers Versus Metal-Organic Frameworks. *Cryst. Growth Des.* **2009**, *9*, 2969−2970.

(4) Roy, M.; Sengupta, S.; Bala, S.; Bhattacharya, S.; Mondal, R. Systematic Study of Mutually Inclusive Influences of Temperature and Substitution on the Coordination Geometry of Co(II) in a Series of Coordination Polymers and Their Properties. *Cryst. Growth Des.* **2016**, *16*, 3170−3179.

(5) Yuan, S.; Feng, L.; Wang, K.; Pang, J.; Bosch, M.; Lollar, C.; Sun, Y.; Qin, J.; Yang, X.; Zhang, P.; et al. Stable Metal−Organic

Frameworks: Design, Synthesis, and Applications. *Adv. Mater.* **2018**, *30*, 1704303.

(6) Sun, J. K.; Yang, X. D.; Yang, G. Y.; Zhang, J. Bipyridinium derivative-based coordination polymers: From synthesis to materials applications. *Coord. Chem. Rev.* **2019**, *378*, 533−560.

(7) Sun, H. L.; Wang, Z. M.; Gao, S. Synthesis, crystal structures, and magnetism of cobalt coordination polymers based on dicyanamide and pyrazine-dioxide derivatives. *Inorg. Chem.* **2005**, *44*, 2169−2176.

(8) Dhers, S.; Wilson, R. K.; Rouzières, M.; Clérac, R.; Brooker, S. A One-Dimensional Coordination Polymer Assembled from a Macrocyclic Mn(III) Single-Molecule Magnet and Terephthalate. *Cryst. Growth Des.* **2020**, *20*, 1538−1542.

(9) Leuenberger, M. N.; Loss, D. Quantum computing in molecular magnets. *Nature* **2001**, *410*, 789−793.

(10) Xu, J.; Bai, Z.; Sun, W. Synthesis and crystal structure of an unprecedented supramolecular complex $[Co(\mu_2\text{-}ClO_4)_2(H_2O)_2]\bullet$ 2MA. *Chin. J. Chem.* **2009**, *27*, 501−504.

(11) Głowacz-Czerwonka, D. Prospects of using melamine solutions in reactive solvents in polymer technology. *Chemik* **2013**, *67*, 289−300.

(12) Peng, W.; Li, H.; Liu, Y.; Song, S. A review on heavy metal ions adsorption from water by graphene oxide and its composites. *J. Mol. Liq.* **2017**, *230*, 496−504.

(13) Winkelmann, J. In *Diffusion in Gases, Liquids and Electrolytes*; Lechner, M. D., Ed.; LANDOLT 3, Vol. *15B1*; Springer Berlin Heidelberg: Berlin, Germany, 2017.

(14) Van Westen, T.; Groot, R. D. Effect of Temperature Cycling on Ostwald Ripening. *Cryst. Growth Des.* **2018**, *18*, 4952−4962.

(15) Reid, R. C.; Sherwood, T. K.; Street, R. E. *Phys. Today* **1959**, *12*, 38−40.

(16) Kahn, O. *Molecular Magnetism*; Wiley-VCH: New York, NY, 1993.

(17) Baca, S. G.; Malinovskii, S. T.; Franz, P.; Ambrus, C.; Stoeckli-Evans, H.; Gerbeleu, N.; Decurtins, S. Synthesis, structure and magnetic properties of cobalt(II) and copper(II) coordination polymers assembled by phthalate and 4-methylimidazole. *J. Solid State Chem.* **2004**, *177*, 2841−2849.

(18) Shi, J.-M.; Chen, J.-N.; Wu, C.-J.; Ma, J.-P. Synthesis, crystal structure and magnetism of 1D cobalt(II) coordination polymer with thiocyanate as bridging ligand. *J. Coord. Chem.* **2007**, *60*, 2009−2013.

(19) Sun, W.-J.; Ke, C.-Y.; Zhang, Q.-Z.; Zhang, X.-L. Syntheses, Crystal Structures and Magnetic Properties of Co(II) Coordination Polymers Based on a Rigid Imidazole Derivative. *J. Inorg. Organomet. Polym. Mater.* **2017**, *27*, 186−193.

(20) Cai, H.; Zou, Y.; Li, Y.; Lian, X.; Tong, X.; Li, J. Structural diversity and magnetic properties of two metal-organic polymers based on bifunctional ligand of 2,5-di(1H-1,2,4-triazol-1-yl)-terephthalic acid. *Inorg. Chem. Commun.* **2019**, *107*, 107499.

(21) Li, J.; Khan, M. R.; Liu, B.; Niu, X.; Li, B.; Hao, Y.; Liu, Z. Synthesis, Structures and Magnetic Properties of CuII and CoII Compounds Based on Asymmetric 5-(1H-Imidazole-1-yl)-3-pyridine Carboxylic Acid. *Eur. J. Inorg. Chem.* **2020**, *2020*, 3786−3796.

(22) Zhang, X. Y.; Xu, M. L.; Wu, J. P.; Wang, J. CRYSTAL STRUCTURE AND PHYSICAL PROPERTIES OF A NEW ONE-DIMENSIONAL POLYMER BASED ON 1,3,5-TRIS(2-METHYL-IMIDAZOL-1-YL)BENZENE AND 5-NITRO-1,3-BENZENEDI-CARBOXYLIC ACID. *J. Struct. Chem.* **2020**, *61*, 1398−1404.

(23) Wei, H.; Huang, H.; Gao, W.; Wang, C.-L.; Liu, J.-P.; Zhang, X.-M. 2D/3D coordination polymers based on di-, tri-, tetranuclear and polymeric chain units with a tricarboxylate ligand: Structures, magnetic and luminescent properties. *Inorg. Chim. Acta* **2020**, *513*, 119944.

(24) Zhou, Y.-H.; Xu, Y.; Shi, J.-Q.; Su, Y.; Sun, M.-L.; Wang, S.-H.; Wang, L.-L.; Wang, Q.-Q.; Wei, Y.-J. Syntheses, structures, and fluorescent and magnetic properties of four metal−organic coordination polymers constructed from dicarboxylate ligands. *Inorg. Nano-Met. Chem.* **2021**, *51*, 1882−1889.

(25) Yin, M.-R.; Yan, Q.-Q.; Li, B.; Yong, G.-P. 1D ladder and 2D bilayer coordination polymers constructed from a new T-shaped ligand: luminescence, magnetic and CO2 gas adsorption properties. *CrystEngComm* **2021**, *23*, 3196−3203.

(26) Zheng, L.-N.; Yan, Y.-T.; Ding, T.; Xue, N. Construction and magnetic properties of cobalt(II) and manganese(II) coordination polymers based on N-heterocyclic carboxylate bifunctional ligands. *Inorg. Chim. Acta* **2021**, *515*, 120054.

(27) Xu, W.-J.; Chen, K.-P.; Zhang, Y.; Ma, Y.; Li, Q.-W.; Wang, Q.-L. Two new Co(II) coordination polymers based on redox-active ligands: Structure, Chromism and Magnetism. *J. Mol. Struct.* **2021**, *1231*, 129948.

(28) Duran, N.; Clegg, W.; Cucurull-Sanchez, L.; Coxall, R.; Jimenez, H.; Moratal, J.; Lloret, F.; Gonzalez-Duarte, P. Unprecedented stabilization of cobalt(II) in a tetrahedral S2O2 environment: The use of a redox-noninnocent ligand. *Inorg. Chem.* **2000**, *39*, 4821−4832.

(29) Miyasaka, H.; Clerac, R.; Campos-Fernandez, C.; Dunbar, K. Metal-metal bonded diruthenium(II, III) assemblies with the polycyano anionic linkers N(CN)(2)(−), C(CN)(3)(−), and 1,4-dicyanamido-2,5-dimethylbenzene (DM-Dicyd(2-)): Syntheses, structures, and magnetic properties. *Inorg. Chem.* **2001**, *40*, 1663−1671.

(30) Marshall, S.; Rheingold, A.; Dawe, L.; Shum, W.; Kitamura, C.; Miller, J. Corner sharing tetrahedral network in Co3(HAT)[N-(CN)]6(OH)2 (HAT = 1,4,5,8,9,12-hexaazatriphenylene). *Inorg. Chem.* **2002**, *41*, 3599−3601.

(31) Tortosa, M.; Mollar, M.; Mari, B.; Lloret, F. Optical and magnetic properties of ZnCoO thin films synthesized by electro-deposition. *J. Appl. Phys.* **2008**, *104*, 033901.

(32) Reger, D. L.; Foley, E. A.; Watson, R. P.; Pellechia, P. J.; Smith, M. D.; Grandjean, F.; Long, G. J. Monofluoride Bridged, Binuclear Metallacycles of First Row Transition Metals Supported by Third Generation Bis(1-pyrazolyl)methane Ligands: Unusual Magnetic Properties. *Inorg. Chem.* **2009**, *48*, 10658−10669.

(33) Ma, L.-F.; Meng, Q.-L.; Wang, L.-Y.; Liu, B.; Liang, F.-P. Multi-dimensional transition-metal coordination polymers with 5-nitro-1,2,3-benzenetricarboxylic acid exhibiting ferro-/antiferromagnetic interactions. *Dalton Trans.* **2010**, *39*, 8210−8218.

(34) Su, Z.; Fan, J.; Chen, M.; Okamura, T.-a.; Sun, W.-Y. Syntheses, Characterization, and Properties of Three-Dimensional Pillared Frameworks with Entanglement. *Cryst. Growth Des.* **2011**, *11*, 1159−1169.

(35) Idešicová, M.; Dlháň, L'.; Moncol, J.; Titiš, J.; Boča, R. Zero-field splitting in tetracoordinate Co(II) complexes. *Polyhedron* **2012**, *36*, 79−84.

(36) Bernini, M. C.; Platero-Prats, A. E.; Snejko, N.; Gutierrez-Puebla, E.; Labrador, A.; Sáez-Puche, R.; Romero de Paz, J.; Monge, M. A. Tuning the magnetic properties of transition metal MOFs by metal-oxygen condensation control: the relation between synthesis temperature, SBU nuclearity and carboxylate geometry. *CrystEngComm* **2012**, *14*, 5493−5504.

(37) Zou, J.-Y.; Shi, W.; Zhang, J.-Y.; He, Y.-F.; Gao, H.-L.; Cui, J.-Z.; Cheng, P. Alkaline cation directed structural diversity of cubic-cage-based cobalt(II) metal-organic frameworks: from pcu to bct net. *CrystEngComm* **2014**, *16*, 7133−7140.

(38) Han, Y.; Song, Y. Novel supramolecular compounds based on tetrathiafulvalene tetracarboxylate with the cationic chains and anionic chains: Syntheses, charactarization and magnetic propertises. *Inorg. Chem. Commun.* **2015**, *55*, 83−87.

(39) Li, L.; Zou, J.-Y.; Gu, Z.; You, S.-Y.; Chen, Y.-H.; Xia, J.; Cui, J.-Z. Two cobalt complexes derived from 1H-1,2,3-triazole-4,5-dicarboxylic acid: Syntheses, structures and magnetic properties. *Inorg. Chem. Commun.* **2016**, *65*, 59−62.

(40) Li, L.; Zou, J.-Y.; You, S.-Y.; Chen, K.-h.; Cui, J.-Z.; Wang, W.-M. Assembly of a new (3,6)-connected cobalt(II) metal−organic framework via a mixed ligands approach. *Polyhedron* **2018**, *141*, 262−266.

(41) Wu, X.-S.; Bao, H.-F.; Zhu, F.-L.; Sun, J.; Wang, X.-L.; Su, Z.-M. Syntheses and magnetic properties of high-dimensional

cucurbit[6]uril-based metal-organic rotaxane frameworks. *Dalton Trans.* **2019**, *48*, 9939−9943.

(42) Boca, R. Zero-field splitting in metal complexes. *Coord. Chem. Rev.* **2004**, *248*, 757−815.

(43) Piwowarska, D.; Gnutek, P.; Rudowicz, C. Origin of the Ground Kramers Doublets for Co 2+(3d 7) Ions with the Effective Spin 3/2 Versus the Fictitious 'Spin'1/2. *Appl. Magn. Reson.* **2019**, *50*, 797−808.

📖 **Recommended by ACS**

Zero-Field SMM Behavior Triggered by Magnetic Exchange Interactions and a Collinear Arrangement of Local Anisotropy Axes in a Linear Co₃ᴵᴵ Complex

Andoni Zabala-Lekuona, Enrique Colacio, *et al.*

NOVEMBER 22, 2023

INORGANIC CHEMISTRY   READ 🔗

Hysteretic Spin Crossover with High Transition Temperatures in Two Cobalt(II) Complexes

Yu-Chen Sun, Xin-Yi Wang, *et al.*

SEPTEMBER 07, 2023

INORGANIC CHEMISTRY   READ 🔗

Site Selectivity for the Spin States and Spin Crossover in Undecanuclear Heterometallic Cyanido-Bridged Clusters

Le Shi, Robert Podgajny, *et al.*

APRIL 25, 2023

INORGANIC CHEMISTRY   READ 🔗

Multi-Technique Experimental Benchmarking of the Local Magnetic Anisotropy of a Cobalt(II) Single-Ion Magnet

Sandeep K. Gupta, Franc Meyer, *et al.*

JANUARY 23, 2023

JACS AU   READ 🔗

Get More Suggestions >